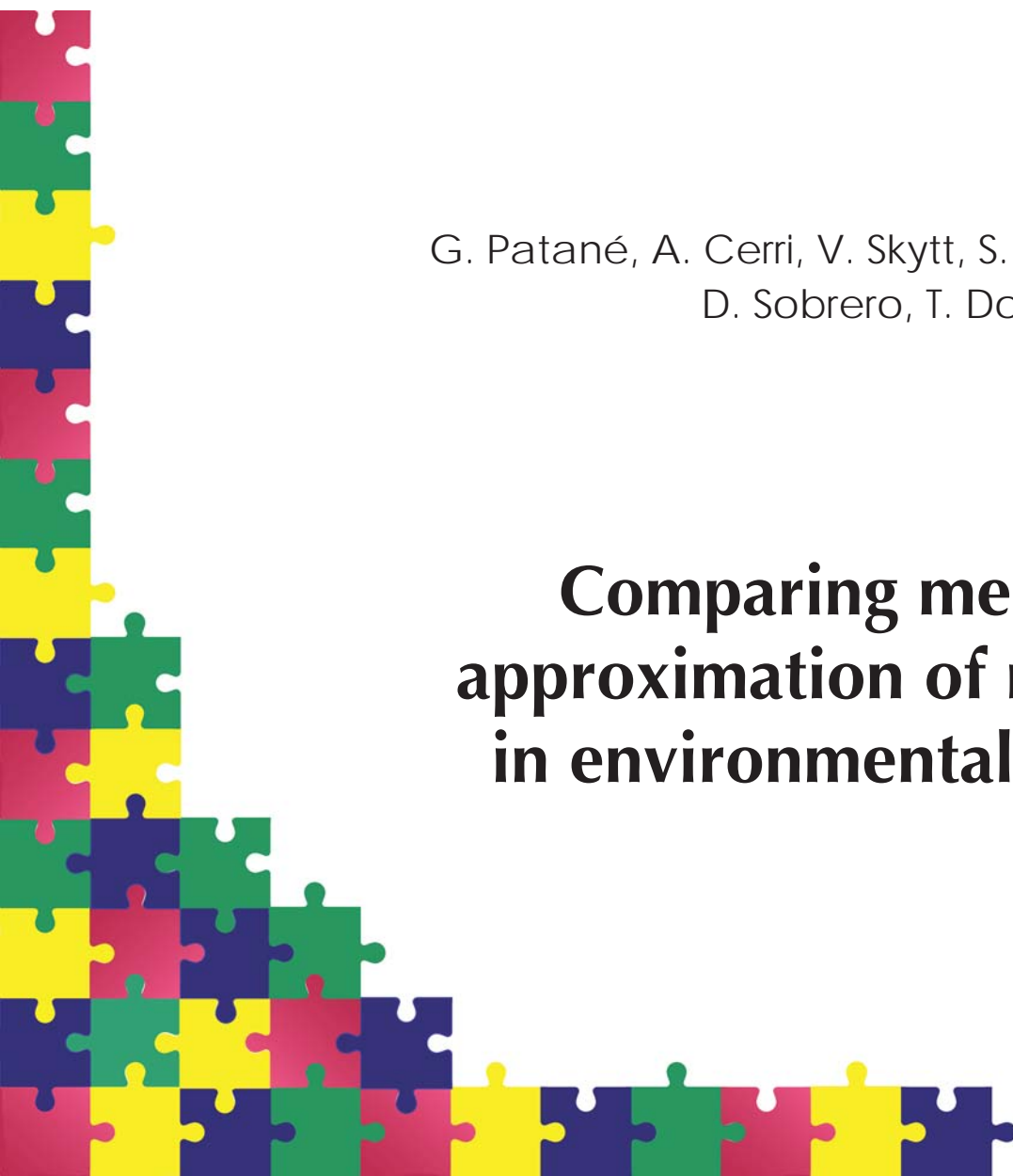


## REPORT SERIES

G. Patané, A. Cerri, V. Skytt, S. Pittaluga, S. Biasotti,  
D. Sobrero, T. Dokken, M. Spagnuolo

# **Comparing methods for the approximation of rainfall fields in environmental applications**



# IMATI REPORT Series

Nr. 16-10 – February 2016

## **Managing Editor**

Annalisa Buffa

## **Editorial Office**

Istituto di Matematica Applicata e Tecnologie Informatiche “E. Magenes”

Consiglio Nazionale delle Ricerche

Via Ferrata, 5/a

27100 PAVIA (Italy)

Email: [reports@imati.cnr.it](mailto:reports@imati.cnr.it)

<http://www.imati.cnr.it>

Follow this and additional works at: <http://www.imati.cnr.it/reports>

---

Copyright © CNR-IMATI, 2016.

IMATI-CNR publishes this report under the Creative Commons Attributions 4.0 license.

## Comparing methods for the approximation of rainfall fields in environmental applications

*G. Patané<sup>a</sup>, A. Cerri<sup>a</sup>, V. Skytt<sup>b</sup>, S. Pittaluga<sup>a</sup>, S. Biasotti<sup>a</sup>,  
D. Sobrero<sup>a</sup>, T. Dokken<sup>b</sup>, M. Spagnuolo<sup>a</sup>*

<sup>a</sup> *CNR-IMATI, Genova, Italy*

<sup>b</sup> *SINTEF, Oslo, Norway*

*Corresponding author:* [michela.spagnuolo@ge.imati.cnr.it](mailto:michela.spagnuolo@ge.imati.cnr.it)



**Abstract.**

Digital environmental data are becoming commonplace and the amount of information they provide is huge, yet complex to process, due to the size, variety, and dynamic nature of the data captured by sensing devices. The paper discusses an evaluation framework for comparing methods to approximate observed rain data, in real conditions of sparsity of the observations. The novelty brought by this experimental study stands in the geographical area and heterogeneity of the data used for evaluation, aspects which challenge all approximation methods. The Liguria region, located in the north-west of Italy, is a complex area for the orography and the closeness to the sea, which cause complex hydro-meteorological events. The observed rain data are highly heterogeneous: two data sets come from measured rain gathered from two different rain gauge networks, with different characteristics and spatial distribution over the Liguria region; the third data set come from weather radar, with a more regular coverage of the same region but a different veracity. Finally, another novelty of the paper is brought by the proposal of an application-oriented perspective on the comparison. The approximation models the rain field, whose maxima and their evolution is essential for an effective monitoring of meteorological events. Therefore, we adapt a storm tracking technique to the analysis of the displacement of maxima computed by the different methods.

**Keywords:** *Surface approximation, Precipitation analysis, Storm tracking*



# Comparing Methods for the Approximation of Rainfall Fields in Environmental Applications

G. Patané<sup>a1</sup>, A. Cerri<sup>a</sup>, V. Skytt<sup>b</sup>, S. Pittaluga<sup>a</sup>, S. Biasotti<sup>a</sup>, D. Sobrero<sup>a</sup>, T.  
Dokken<sup>b</sup>, M. Spagnuolo<sup>a</sup>

<sup>a</sup> *CNR-IMATI, Genova, Italy -*

*(patane,cerri,pittaluga,biasotti,sobrero,spagnuolo)@ge.imati.cnr.it*

<sup>b</sup> *SINTEF, Oslo, Norway - (vibeke.skytt,tor.dokken)@sindef.no*

---

## Abstract

Digital environmental data are becoming commonplace and the amount of information they provide is huge, yet complex to process, due to the size, variety, and dynamic nature of the data captured by sensing devices. The paper discusses an evaluation framework for comparing methods to approximate observed rain data, in real conditions of sparsity of the observations. The novelty brought by this experimental study stands in the geographical area and heterogeneity of the data used for evaluation, aspects which challenge all approximation methods. The Liguria region, located in the north-west of Italy, is a complex area for the orography and the closeness to the sea, which cause complex hydro-meteorological events. The observed rain data are highly heterogeneous: two data sets come from measured rain gathered from two different rain gauge networks, with different characteristics and spatial distribution over the Liguria region; the third data set come from weather radar, with a more regular coverage of the same region but a different veracity. Finally, another novelty of the paper is brought by the proposal of an application-oriented perspective on the comparison. The approximation models the rain field, whose maxima and their evolution is essential for an effective monitoring of meteorological events. Therefore, we adapt a storm tracking technique to the analysis of the displacement of maxima computed by the different methods.

---

## 1. Introduction

The large amount of digital data provides an extremely rich, yet difficult to process, amount of information about our environment, geographic and meteorological phenomena. The geographical area selected for presenting our results, the Liguria

region in Italy, is an exemplary case study: the articulated orography is characterized by many small catchment basins that are highly influenced by local maxima of precipitation. Moreover, the proximity to the sea causes additional problems during storms, concurring to the creation of secondary low pressure areas, also known as the *Genova Low*, which increases the amount of precipitation and the risk of critical flash floods. The continuous observation of rain data during critical events, as well as the analysis of historical time series of precipitation, are definitely crucial to support a better understanding and monitoring of hydro-geological risks, such as floods and landslides (Keefer et al., 1987; Hong et al., 2007; Wake, 2013; Hou et al., 2014). A robust approximation method, resilient to errors, is therefore highly desirable.

In this context, the paper presents the results of the evaluation of three approximation techniques, which give insights into their suitability to capture the behaviour of precipitation events: LR (Locally Refinable) B-Splines and meshless approximation with kriging, and Radial Basis Functions (RBFs). The comparison of methods for rainfall approximation has been addressed in the literature both at the theoretical level (Scheuerer et al., 2013) and for domain-specific analysis (Skok and Vrhovec, 2006). Our study contributes to this topic extending the analysis to another approximation technique, LR B-Splines, and using a new setting for the comparison, inspired by the theory of *topological persistence* (Edelsbrunner et al., 2002). The basic idea is that in order to characterize precipitation events, it is important to focus on the main features of the rainfall fields and their configuration, discarding irrelevant details that do not contribute to understanding the overall event structure. With this motivation in mind, the *prominence* of precipitation maxima is measured through the notion of *persistence*, which allows for hierarchically organize maxima by importance, and possibly filter out irrelevant (i.e., non-prominent) ones. Based on this discussion, we developed a criteria to compare different approximation methods based on the analysis of the number and location of the most prominent maxima they produce.

Finally, we remark the focus on the evaluation of approximation performance in real conditions of sparsity: the number of the measuring gauges is quite low with respect to the area covered and their distribution is quite uneven. The evaluation results give also insights on the influence of integrating radar data in the approximation: rain data extracted from radar measures provide a complementary information with respect to rain gauges, less accurate but with a wider and more stable coverage. The integration of measured rain and radar data makes give insights on the reliance on radar-driven approximations in case of failures of some rainfall stations during heavy storms.

For this study, we considered LR B-Spline and two meshless approximation, krig-

ing and radial basis functions. The reason for this choice is to understand the performance of approximation methods, LR and RBF, which have been used mostly in computer graphics up to now, but which have interesting properties for this application. Kriging has been selected as well as it is among those most widely used in the application domain, together with other methods such as the inverse distance weighting. The latter, moreover, seems to be less performant to the specific case studies (sparsity conditions), while other possible choices as the Poisson interpolation could cause a too high smoothing effects; in both cases, we know a-priori that many details are lost.

LR B-Splines are particularly useful as a compact representation of functions over large domains: they use a (locally) regular domain parameterization and can be locally refined according to the required approximation error. Ordinary kriging is a very well-known approximation method which uses a variogram capturing the spatial distribution of the data. Similarly, RBFs use a kernel, which can be also adapted to the spatial distribution of the data, through the selection of the kernel width. The three approximation methods define slightly different functions, whose behaviour is studied both at the numerical level (accuracy, sensitivity to sparseness, computational issues) and at a qualitative level by measuring the differences among the configuration of precipitation maxima induced by the three techniques.

The comparative study was conducted selecting Liguria as area of interest, and two precipitation events recorded on September 29, 2013 and January 17, 2014, characterized by different meteorological situation and events. For the latter event, we also used rain data extracted from weather radar acquisition.

To contextualize better the comparison, we start with a short overview of related work on rain observation methods, approximation and comparison techniques (Sect. 2). We present the setting adopted for the evaluation with details on the rain event and metrics used for the comparison (Sect. 3). We give the formal definition of the three approximation methods discussed (Sect. 4) and discuss their performances with respect to accuracy, behaviour with respect to sparsity, and computational aspects (Sect. 5). Then, the approximation schemes are compared by analyzing the difference in the configuration and prominence of the detected maxima (Sect. 6). Finally (Sect. 7), we summarize our study.

## 2. Related work

*Measuring rainfall data.* Rainfall intensities are traditionally derived by measuring the rain rate through rain gauges, weather radar, or by measuring the variations in soil moisture with micro-wave satellite sensors (Brocca et al., 2014). Even though

satellite precipitation analysis allows the estimation of rainfall data at a global scale and in areas where ground measures are sparse, the evaluation of light rainfalls is generally difficult, thus generating an underestimation of the cumulated rainfalls (Kucera et al., 2013). To bypass this issue, in (Brocca et al., 2014) the soil water balance equation is applied to extrapolate the daily rainfall from soil moisture data. The integration of rainfall data at regional and local levels is also intended to provide a more precise approximation of the underlying phenomenon on urban areas, which are sensitive to spatial variations in rainfalls (Segond, 2007). The combined use of rain height measured at rain gauges and radar-derived ones provides locally accurate but spatially anisotropic measures (around gauges) with globally distributed detailed data. Furthermore, we mention that the spatial and temporal variations (e.g., speed, direction) of rainfalls are important to characterize their variability and peaks, together with their effects on catchments.

*Approximating rainfall data.* Different approaches have been used for the approximation of rainfall data. In (Thiessen, 1911), rainfalls recorded in the closest gauge are associated with unsampled locations, by identifying a Voronoi diagram around each weather station and assigning the measured rainfall to the respective Voronoi cell. Back to the 1972, the U.S. National Weather Service proposed to estimate the unknown rainfall values as a weighted average of the neighbouring values; the weights are the inverse of the squares of the distances between the unsampled locations and each rainfall sample. The underlying assumption is that the samples are autocorrelated and their estimates depend on the neighbouring values. This method has been extended in (Teegavarapu and Chandramouli, 2005) through the modified inverse distance and the correlation weighting method, the inverse exponential and nearest neighbour distance weighting method, and the artificial neural network estimation. In (McRobie et al., 2013), storms are modelled as clusters of Gaussian rainfall cells, where each cell is represented as an ellipse whose axis is in the direction of the movement and the rainfall intensity is a Gaussian function along each axis (Willems, 2001).

McCuen (McCuen, 1989) proposed the *isoyetal method* that allows the hydrologists to take into account the effects of different factors (e.g., elevation) on the rainfall field by drawing lines of equal rainfall depths among the rain-gauges and taking into account the main factors that influence the distribution of the rain field. Then, the rainfalls at new locations are approximated by interpolation starting from the isohyets. Geo-statistical approaches allow us to take into account the spatial correlation between neighboring samples and to predict the values at new locations (Journel and Huijbregts, 1978; Goovaerts, 1997, 2000). Furthermore, the geo-statistic estimator includes additional information, such as weather-radar data (Creutin et al., 1988;

Azimi-Zonooz et al., 1989) or elevation from a digital model (Goovaerts, 2000; Di Piazza et al., 2011).

For our experimental study, we selected kriging as the representative of the best-known and widely used methods. Also, we decided not including the inverse distance weighting and the Poisson interpolation, respectively, for the low and high smoothness of the resulting interpolating function. Instead, we decided to experiment and compare two methods that have not been applied, to our knowledge, in this application domain already, to see if they could bring new insights or provide a more robust handling of highly dynamic and complex events as those observed in Liguria.

*Comparing rainfall data approximations.* For the comparison of the precipitation fields originated from different approximation schemes, we have adopted a number of standard metrics to assess their differences. Moreover, we have extended the evaluation approach by comparing the differences in the configurations of meaningful features of the precipitation fields, namely prominent maxima. The motivation for this evaluation is that precipitation maxima convey important information for *storm tracking*, a crucial analysis of dynamic measures of rain data, where meaningful features associated with distinct time frames, are matched to track their evolution along time.

There is a rich and interesting literature on storm tracking, mostly using a region-based approach, where regions in radar images are characterized by high reflectivity and sufficiently large area. Various characteristics of these regions, such as centroids, area, major/minor radii, and orientation, are computed, see for instance (Lakshmanan and Smith, 2009; Dixon and Wiener, 1993; Han et al., 2009). However, we underline that the focus of the paper is not storm tracking. Indeed, we use the storm tracking measure recently proposed in Biasotti et al. (2015) for the comparison of the different fields. The approach is based on a topological analysis of rainfall data, which focuses on the most prominent precipitation maxima instead of regions. Indeed, the granularity of the analysis is more appropriate for the characteristics of the geographic area selected; at the same time, the introduction of an ad-hoc distance, combining geographical distance and the measured rainfall difference, allows for matching and tracking prominent maxima along time. The same strategy for matching maxima is used in this paper to evaluate the displacement of the maxima of the different approximated fields, treating them as if they were snapshots at different times.

### 3. Case studies and evaluation metrics

The area selected for the evaluation is the Liguria region, in the north-west of Italy. Liguria can be described as a long and narrow strip of land, squeezed between the sea, the Alps and the Apennines mountains, with the watershed line running at an average altitude of about 1000 m. The orography and the closeness to the sea make this area particularly interesting for hydro-meteorological events, frequently characterized by heavy rain due to Atlantic low pressure area, augmented by a secondary low pressure area created by the Ligurian sea (Genova Low). Moreover the several and small catchments are causing fast flooding events, and even small rivers exhibit high hydraulic energy due to the quick variation of altitude. This is the main motivation behind our analysis, which targets the understanding of the best approximation method to capture important and potentially dangerous precipitation events.

#### 3.1. *Rainfall stations and radar data*

In Liguria, observed rainfall data are captured by two different rain gauges networks. The first rain gauge network is owned by the ARPAL team of Regione Liguria, and consists of 143 professional measure stations distributed over the whole region; the measures are acquired every 5-20 minutes, and the stations are connected by GPRS and radio link connection, producing about 2 MB data per day. The second rain gauge network is owned by the Genova municipality and consists of 25 semi-professional measuring stations spread within the city boundary; the acquisitions are done every 3 minutes, and the stations are linked by GPRS or LAN connections, with an average production of 1Mb data per day. The configuration of the rain gauge networks is shown in Fig. 1.

The two rain gauge networks act as sampling devices of the true precipitation field, working at two different scales, that is, at two different spatial and temporal distributions. Since the temporal interval is different for each network, we have cumulated the station rainfalls to a step of 30 minutes. This selection is also motivated by the desire to produce a fine-grained evaluation of the approximation methods in the perspective of a real-time precipitation monitoring. Note that the cumulated interval is a much smaller than the one used in (Skok and Vrhovec, 2006), where an interval of 24 hours was used. Concerning the precipitation events, we selected two different rainy days, September 29, 2013 and January 17, 2014. The first was characterized by light rain over the whole Liguria and 2 different rainstorms that caused local flooding and landslides, without damages. The second was characterized by the transit of different fronts with well distributed rain, and was part of a rainy period that caused several deaths and a train derail. The maximum rain-rate over all time

step is  $60\text{mm}/30'$  and the average rain-rate is  $1.12\text{mm}/30'$ . For the second event, we also used the rainfall measured every 10 minutes provided by the polarimetric weather radar of Liguria, deployed by ARPAL. The radar scans cover an area of about 134km, and the rainfall measures extracted from the scan are sampled on a grid with 1 km of resolution.

In addition to real data, we adopt also a synthetic rain field as an additional ground-truth defined using a module of the GRASS-GIS software, which produces a fractal field based on spectral synthesis methods (Saupe, 1988) (Fig. 2). The generated values have been scaled to be in the range of the rainfall values. To simulate a set of rain gauges, we sample the synthetic rainfall field with 200 points, randomly placed in a grid that contains Liguria. The goal here is to evaluate how the fields obtained with the three methods are far from the synthetic one in the whole grid.

### 3.2. Evaluation settings

To establish a formal evaluation setting, let us formulate the problem of rainfall approximation as follows. Given a set of points  $\mathcal{P} := \{\mathbf{p}_i\}_{i=1}^n$ , let us call  $f : \mathcal{P} \rightarrow \mathbb{R}$  the precipitation field, known only at the  $n$  sample points in  $\mathcal{P}$ , which represent the positions of the measurement instruments and/or the nodes of the regular grid associated with the radar image. An approximation of  $f$  is defined as  $F : \mathbb{R}^2 \rightarrow \mathbb{R}$  such that  $d(F(\mathbf{p}) - f(\mathbf{p})) \leq \epsilon$  for some required distance  $d(\cdot, \cdot)$  and threshold  $\epsilon$ . When  $d(F(\mathbf{p}) - f(\mathbf{p})) = 0$  the approximation is an interpolation of  $f$ . The map  $F$  can be used to evaluate the value of the precipitation at any point other than those in  $\mathcal{P}$ , with results differing according to the approach used to define  $F$ . In our case, we will consider three different  $F$  approximation functions.

To compare the approximations, we adopt a cross-validation strategy, exploiting the sets of data we have at regional and municipality level. Every rainfall station at  $\mathbf{p}_i$  is iteratively turned off, that is, it is not used in the computation of  $F$ ; the resulting approximation function  $F$  is sampled at that position  $\mathbf{p}_i$  and compared with the rain value measured at  $\mathbf{p}_i$ , which acts as a ground truth (leave-one-out strategy). Then, the rainfall data measured by the municipality stations are used as ground-truth to validate the values approximated from the ARPAL data set: in this setting, the cross-validation aims at evaluating the capability of the different methods to estimate the local features of rain fields interpolated over a sparse data set, with different spatial distribution.

The comparative study also includes the analysis of the spatial configuration of local maxima extracted from the rainfall fields produced by each approximation scheme. In this case, local maxima are endowed with a notion of prominence bor-

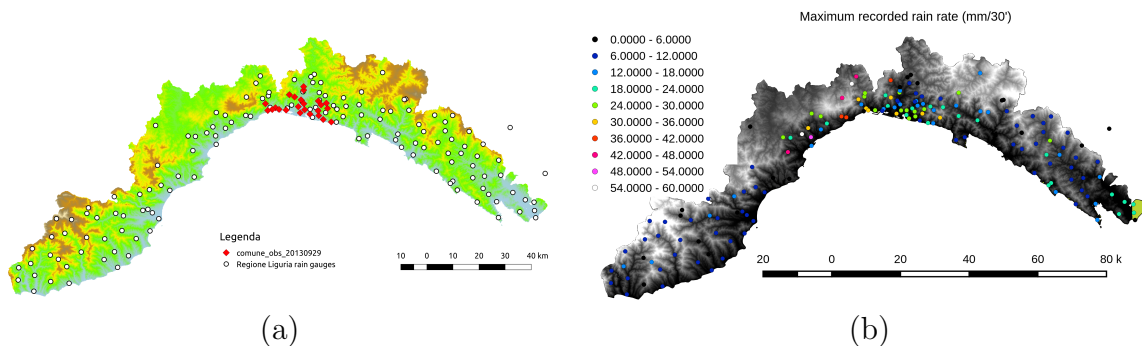


Figure 1: (a) Input rainfall measures at 143 stations (regional level, white points) and 25 stations (municipality level, red circles). (b) Map of the maximum rain rate recorded at each weather station, which highlights that only the central west of the region has been involved by heavy rain and the remaining part were interested by drizzle.

rowed from topological persistence, which is used to quantify the importance that a maximum has in characterizing the associated rainfall field.

For this set of experiments, the approximated precipitation fields were discretized at the vertices of a digital terrain model, which is coming from the SRTM (Shuttle Radar Topography Mission (Farr et al., 2007)), available in public domain at the URL <http://www2.jpl.nasa.gov/srtm/>, and with a spatial resolution of 100 mt.

## 4. Theoretical background

In the following, we give an overview of the three approximation methods compared and of the persistence analysis framework used to analyse the evolution of precipitations.

### 4.1. Approximation schemes

*LR B-Splines.* The rainfall values are parameterized on the  $xy$ -values of the corresponding geographic location and the rainfall is approximated by a 2.5D LR B-spline surface (Dokken et al., 2013). Similar to tensor product B-spline surfaces, the LR B-spline surfaces are defined from basis functions (B-splines) which have local support. The approximation of the rainfall data is performed by an iterative procedure starting from a lean tensor-product B-spline surface being constantly equal to zero. For each iteration the distance between the current surface and the rainfall data is computed, the surface is refined locally where a given tolerance is not met, and the surface coefficients are updated using *Multilevel B-spline approximation (MBA)* (Lee et al., 1997) adapted for LR B-splines. The MBA method is a local and explicit approximation method, where the surface coefficients are updated based on the data



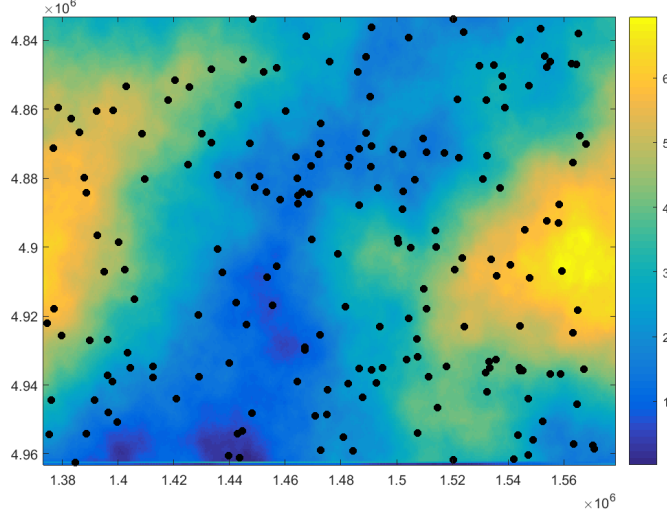


Figure 2: The synthetic field and the position of the 200 random rain gauges (black dots) used as ground truth for the evaluation of the approximation schemes. The values of the field varies from 0 (blue) to 6.94 (yellow)

points situated in the support of the corresponding B-spline. The performance depends on three components, which are done at each iteration step: refinement of the LR B-spline, distance computations, and update of the surface coefficients. The latter two elements are the most time consuming. For each iteration, the coefficients are updated twice and one additional distance computation is performed. Let the number of data points be  $N$ . The number of non-zero B-splines for each data point varies, but will be in the magnitude of  $(d_1 + 1) \times (d_2 + 1)$  where  $d_1$  and  $d_2$  are the polynomial degrees in the two parameter directions of the surface. The surface is bi-quadratic so  $d_1 = d_2 = 2$ . In our tests, the algorithm is run with 20 iterations giving a total of  $3 \times 20 \times N \times 9$  bi-variate B-spline evaluations.

*Implicit approximation with Radial Basis Functions.* The implicit approximation computes the map  $F(\mathbf{p}) := \sum_{i=1}^n \alpha_i \varphi_i(\mathbf{p})$  as a linear combination of the basis  $\mathcal{B} := \{\varphi_i(\mathbf{p}) := \varphi(\|\mathbf{p} - \mathbf{p}_i\|_2)\}_{i=1}^n$ , where  $\varphi$  is the kernel function (Aronszajn, 1950; Dyn et al., 1986; Micchelli, 1986; Patanè et al., 2009). Depending on the properties of  $\varphi$ , we distinguish globally- (Carr et al., 2001; Turk and O’Brien, 2002) and compactly- (Wendland, 1995; Morse et al., 2001) supported radial basis functions. Then, the coefficients  $(\alpha_i)_{i=1}^n$  solve a  $n \times n$  linear system, which is achieved by imposing the interpolating constraints  $F(\mathbf{p}_i) = f(\mathbf{p}_i)$ ,  $i = 1, \dots, n$ . Since a  $n \times n$  linear system is solved once, the computational cost of the approximation with globally- and locally-

supported RBFs is  $O(n^3)$  and  $O(n \log n)$ , respectively. In our experiments, we have chosen the Gaussian kernel  $\varphi(st) := \exp(-st)$ , which has a global support; in fact, its fast decay makes it suitable to approximate rainfalls with a sparse spatial distribution and that change quickly in time. To this end, the width of each basis function is automatically adapted to the local sampling density by selecting its width according to the local spatial distribution of the rainfall stations (Dey and Sun, 2005; Mitra and Nguyen, 2003).

*Kriging.* The previous two approximation methods do not take into account in an explicit manner the correlation among observations, which may have unwanted effects especially in the case of unevenly distributed observations. Furthermore, there is no natural mechanism for propagating the individual quality of the observations into a quality description of the estimation. A class of methods that takes care of these issues is kriging, (Wackernagel, 2003), which is a common technique in environmental sciences and a special case of the maximum likelihood estimation. The underlying assumptions are that the quality of the observations is given as variance values, and that the covariance between observations only depends on their mutual spatial or temporal distance, and not on their location. Formally, kriging is expressed as  $F(\mathbf{p}) := \sum_{i=1}^n \omega_i f(\mathbf{p}_i)$ , where the weights  $\omega := (\omega_i)_{i=1}^n$  are the solution to the linear system  $\mathbf{C}\omega = \mathbf{d}$ , where  $\mathbf{C}$  is the covariance matrix of the of the input points,  $\mathbf{d}$  is the array of the covariance between the positions of the rainfall stations and the points that belong to a neighborhood of the sample point. The covariance is expressed by the variogram model, which reflects the priors on the spatial variability of the values. The main problem with kriging is the low computational efficiency, as the solution of the linear systems scales quadratically with the number of observations. In the implementation used, the problem is addressed by combining kriging with deterministic spatial division techniques, which efficiently restrict the number of observations to the closest ones. More specifically, the  $Kd$ -tree is used to select only the 20 closest neighbors for the matrix inversion and in our tests we have used a constant variogram, whose nugget is set equal to 10% and the range is 30 Km. Fig. 4 shows the results obtained by kriging when radar rain data are integrated.

#### 4.2. Prominent rainfall maxima via persistence analysis

The importance of precipitation maxima is evaluated by means of the *persistence analysis*. Given a scalar field  $F : \mathcal{M} \rightarrow \mathbb{R}$  (e.g., the interpolated rainfall field), persistence analysis is used to study the evolution of the connectivity in the superlevel sets  $\mathcal{M}^t = \{\mathbf{p} \in \mathcal{M} : F(\mathbf{p}) \geq t\}$ , for  $t \in (-\infty, +\infty)$ . Sweeping  $t$  from  $+\infty$  to  $-\infty$ , new connected components of  $\mathcal{M}^t$  are either born, or previously existing ones are merged together. A connected component  $C$  is associated with a local maximum  $\mathbf{p}$

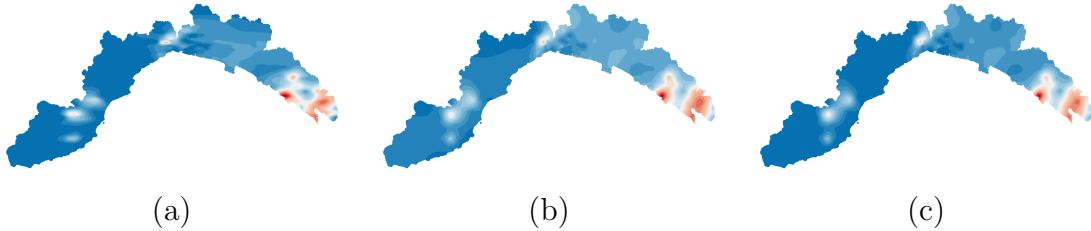


Figure 3: Rainfall fields computed for the event of September, 23: (a) LR B-Spline, (b) RBF, (c) Kriging. Colors represent the field values from low (blue) to high (red).

of  $F$ , where the component is first born. The value  $F(\mathbf{p})$  is referred to as the birth time of  $C$ . When two components corresponding to local maxima  $\mathbf{p}_1, \mathbf{p}_2$ , with  $F(\mathbf{p}_1) < F(\mathbf{p}_2)$ , merge together, we say that the component corresponding to  $\mathbf{p}_1$  dies. In this case, the component associated with the smaller local maximum is merged into that associated with the larger one. Each local maximum  $\mathbf{p}$  of  $F$  is associated with its *persistence value*  $\text{pers}_F(\mathbf{p})$ , which is defined as the difference between the birth and the death level of the corresponding connected component. Maxima associated with a higher persistence value identify relevant features and structures of the underlying phenomena, while maxima having a low persistence value are interpreted as local information or noise, see Figure 5 for a visual intuition.

To compute the local maxima and the associated persistence values,  $F$  is interpolated on the vertices of a triangle mesh  $\mathcal{M}$ . The points of  $\mathcal{M}$  are first sorted in decreasing values, from  $\max F$  to  $\min F$ ; then, the classical 0th-persistence algorithm (Edelsbrunner et al., 2002; Edelsbrunner and Harer, 2010) is used. The cost of sorting the  $n$  points of  $\mathcal{M}$  is  $O(n \log n)$ ; after sorting, by using a union-find data structure the persistence algorithm requires linear storage and running time at most proportional to  $O(m\alpha(m))$ , where  $m$  is the number of edges in the mesh and  $\alpha(\cdot)$  is the inverse of the Ackermann function. An example for the extraction of local maxima at three different persistence levels is given in Fig. 6.

## 5. Approximation behavior

The first set of results that we discuss is related to the comparison of the behaviour with respect to approximation performance and computational complexity. Concerning the leave-one-out cross-validation strategy, we have checked the results by computing the three approximation fields turning off, iteratively, each rainfall station at  $\mathbf{p}_i$ , for each cumulated interval. The value of the approximation function  $F$  obtained was then compared at  $\mathbf{p}_i$  with the rain value measured by the corresponding

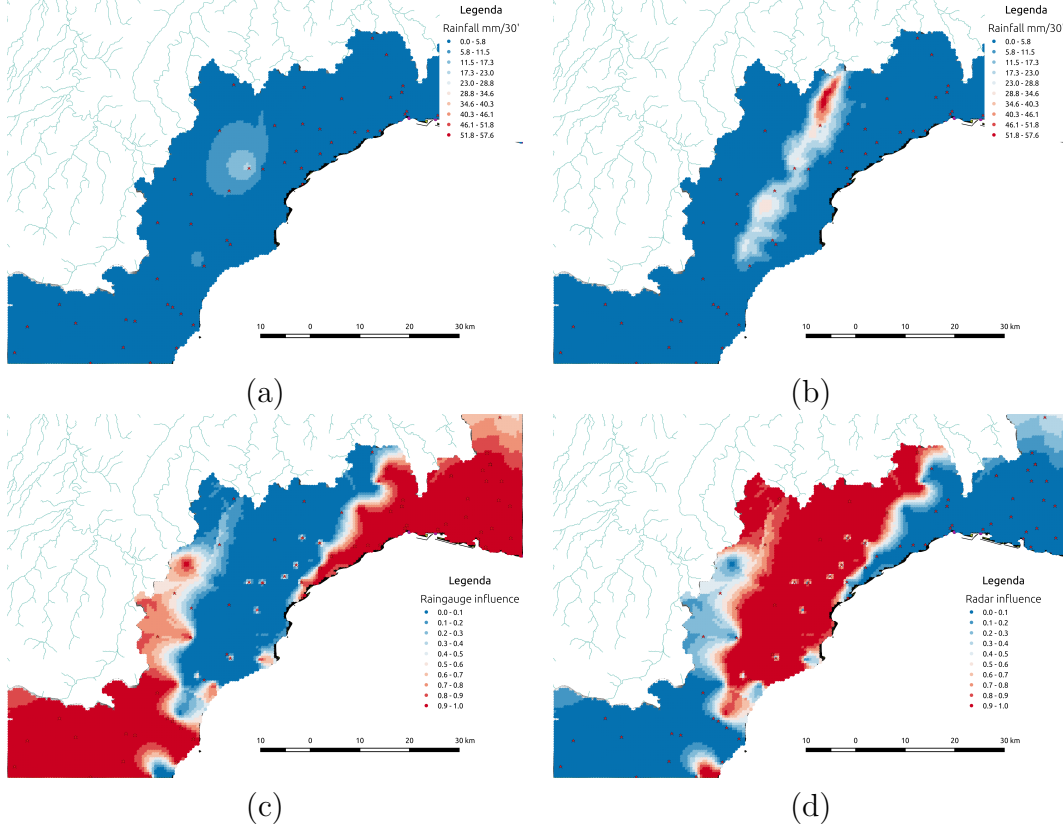


Figure 4: Ordinary kriging approximation of rainfalls computed with (a) rain gauges and (b) integrated with radar measurements. (c) Rain gauges weights and (d) radar data set mapped in (b). Colors represent the field values from low (blue) to high (red).

rain gauge at  $\mathbf{p}_i$ , acting as a ground truth. The statistics of the evaluation are shown in Table 1; the approximation methods behave in a slightly different way depending on the three scenario. In the synthetic and the day-2 case studies, the best performances are achieved by RBFs and LR B-splines, while ordinary kriging has a larger maximum error in the synthetic case and larger mean absolute error for day-2. In the day-1 case study, ordinary kriging and LR B-Splines have a smaller maximum error, but the RBFs have a smaller mean-squares error and standard deviation. In Fig. 7, the plot of the MSE distribution for the three methods is shown, per each time interval. The MSE has been computed taking into account all datasets for all tests. The plot is related to the day-1 event.

The histogram of the error in the Fig. 8 shows clearly that the distribution of ordinary kriging is normally distributed while RBF has positive skewness and LR

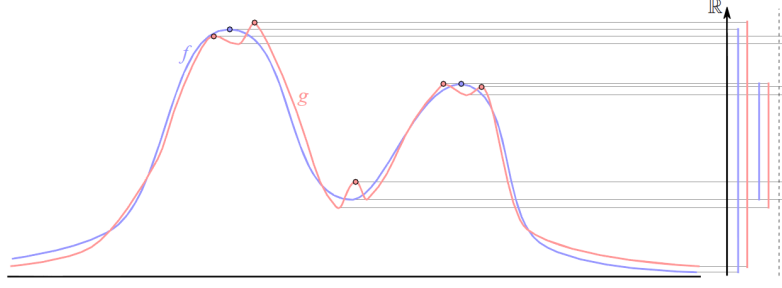


Figure 5: Two scalar fields  $f$ ,  $g$  and their local maxima. On the right, pictorial representation for the persistence of each local maxima. Segments on the right of the dotted line stand for the persistence of topological noise.

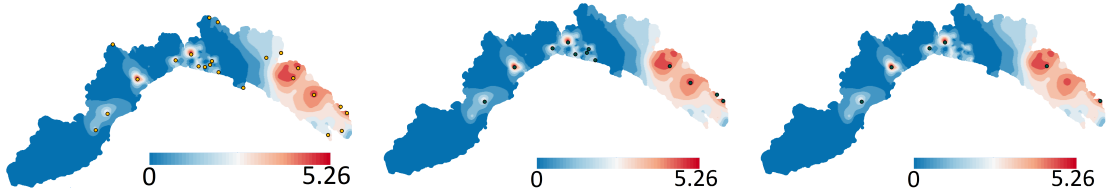


Figure 6: A function  $F : \mathcal{M} \rightarrow \mathbb{R}$ , color-coded from blue (low) to red (high) values, and the associated local maxima having persistence greater than  $\alpha(\max F - \min F)$ , with  $\alpha = 0.05, 0.15$  (middle) and  $0.25$ .

B-spline has a negative skewness. The global behaviour of the three approximation algorithms is also well shown in the map depicted in Fig. 9, the distance between the approximated fields and synthetic ground truth are plotted: ordinary kriging produces more spots that are characterized by an error higher than RBF and LR B-spline.

The second set of results concerns the cross-validation with the rainfall data measured by the municipality stations as ground-truth to validate the values that approximate only the ARPAL data set. This validation aims at gathering indicators on the behavior, in terms of accuracy, on different spatial distribution of the sample points. This approach is meaningful as the two observation networks cover an overlapping region of the study area. The network from Genova municipality is located within the boundary of the city and is denser than the ARPAL one, which covers the whole study area, and some of the ARPAL stations are located in the Genova municipality. Comparing the approximation results at these two scales, we have evaluated the sensitivity of the approximation to local distributions of the samples and the capability to estimate the local features of rain fields interpolated over a sparser data set. According to the results in Table 2, ordinary kriging and LR B-Splines

Method	Max [mm]	Mean [mm]	Median [mm]	Std. dev. [mm]	MSE [mm <sup>2</sup> ]
<i>Syntethic</i>					
Ord. krig.	0.93 (14.1%)	0.15	0.10	0.22	0.04
RBFs	0.55 (8.3%)	0.14	0.10	0.18	0.03
LR B-Splines	0.48 (7.1%)	0.16	0.11	0.22	0.05
<i>Day 1</i>					
Ord. krig.	32.44 (54.1%)	0.02	5.85E-05	2.38	5.64
RBFs	37.80 (63.0%)	0.97	0.34	2.12	5.44
LR B-Splines	27.2 (45.3%)	-0.04	1.20E-5	2.73	7.05
<i>Day 2</i>					
Ord. krig.	16.6 (88.3%)	1.95	1.18	2.88	8.61
RBFs	16.59 (88.3%)	1.28	0.80	1.97	3.88
LR B-Splines	16.6 (88.3%)	1.27	0.79	1.98	3.95

Table 1: Statistics for the error distribution of the cross validation.

Method	Max [mm]	Mean [mm]	Median [mm]	Std. dev. [mm]	MSE [mm <sup>2</sup> ]
Ord. krig.	28.62 (47.7%)	0.59	3.26E-3	4.45	20.21
RBFs	36.77 (61.2%)	1.41	0.44	3.25	12.58
LR B-Splines	30.39 (50.6%)	0.59	3.71E-3	4.45	20.19

Table 2: Statistics for the error distribution of the accuracy evaluation at different scales for day 2.

have the smaller maximum error, but the RBFs have a smaller mean-squares error.

### 5.1. Local analysis of the field differences

Now, we compare the rainfall approximations looking at the differences of the rain values assumed on the DTM and the local smoothness of the three fields. First, we show the point-wise difference of the rainfall fields (Fig. 10). As expected, the difference of the fields is zero at the rain stations and, for the radar data also in the nodes of the regular grid. Since for the kriging approximation we adopted a local support, it gives a slightly perturbed approximation of the field far from the rain gauges and the radar nodes. Furthermore, the approximations with LR B-Splines and RBFs have a smoother behaviour and a lower approximation error.

To measure the smoothness of the approximated rainfall fields, we compare the corresponding normalized gradients (Fig. 11). More precisely, given the approximated rainfall fields  $F_1$ ,  $F_2$  and the gradients  $\nabla F_1$  and  $\nabla F_2$ , their point-wise difference at the node  $(i, j)$  of a uniform grid contained in the bounding box of Liguria is

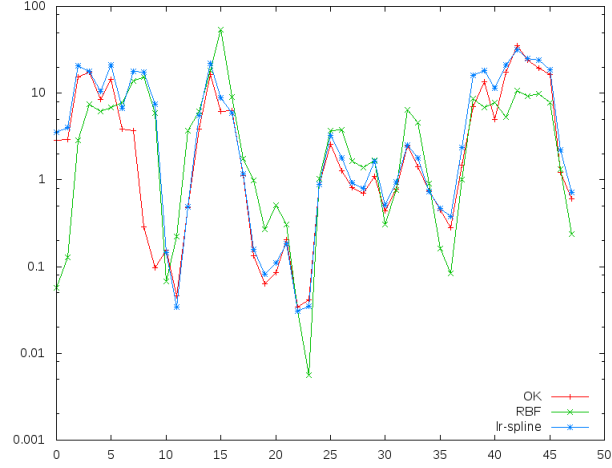


Figure 7: Leave-one-out cross validation for day 2:  $y$ -axis reports the MSE [ $mm^2$ ] for each time step  $x$ -axis.

measured as Biasotti et al. (2007)

$$d(\nabla F_1, \nabla F_2)(i, j) := 1 - |\langle \nabla F_1(i, j), \nabla F_2(i, j) \rangle_2|.$$

As expected, the behaviour of the gradients and their dot product reflects the punctual difference of the rainfall fields. Fig. 12 represents the difference of the gradients over the selected grid: it can be seen that kriging has noisy values far from the sampling points, as a matter of the local behaviour of the algorithm; RBF and ordinary kriging behave in a similar way near the samples while LR B-Spline show difference in the gradient with respect to both other methods.

### 5.2. Computational complexity

The computational complexity of the different algorithms has been tested over a 64 bits workstation 8 cores at 1.6GHZ and RAM of 16 GB. The system runs an Ubuntu 14.04LTS with 3.13.0 kernel. The computational time is measured on the rainfall data from the first day and with only rain gauges (no radar). The run of LR B-Splines takes 19.33 seconds to compute the approximation over the whole region (20K points) for the 48 time intervals. For the same task, the ordinary kriging takes 1.746 seconds and RBFs approximation takes 6.23 seconds. One important point to make here is that, for all the methods, the computational complexity and the timing collected are well below the time interval analyzed (30min). This important characteristic tells us that we could use any of them for real-time monitoring of

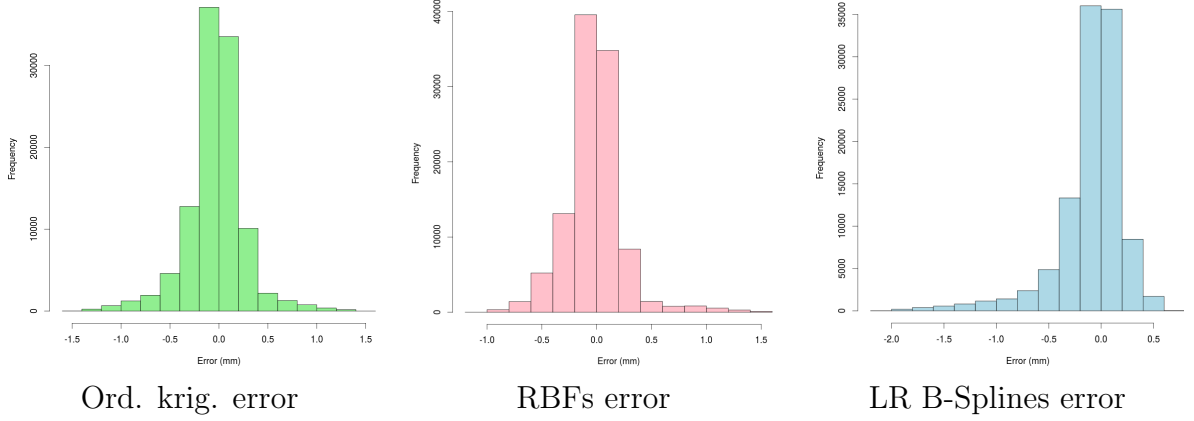


Figure 8: Histograms of the differences among the three approximated rainfall fields and a synthetic ground truth.

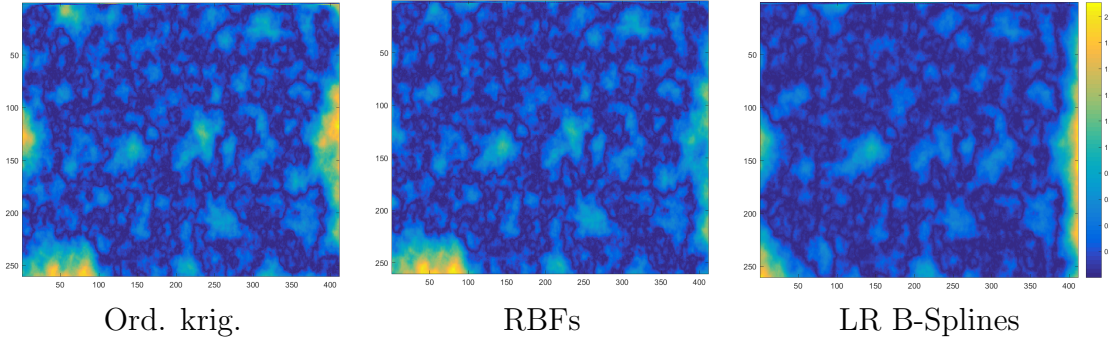


Figure 9: Error between the three approximated fields and the synthetic ground truth.

the rain events. The analysis carried on until now does not tell us much about the scalability of the methods for a larger set of observation points, where the computational complexity could become an issue.

## 6. Persistent rainfall maxima

Tables 3-6 report the comparative results about the extraction of persistent maxima when considering the rainfall fields produced by the three approximation schema using the ARPAL rainfall stations and when these stations are integrated with the radar data. For these tests, we used the rain data of the first precipitation event and radar data (see Sect. 3). Hence, for each approximation scheme, we considered the 48 approximated fields, one for each cumulative step. For each field  $F$ , the associated persistence maxima have been extracted according to four different values for



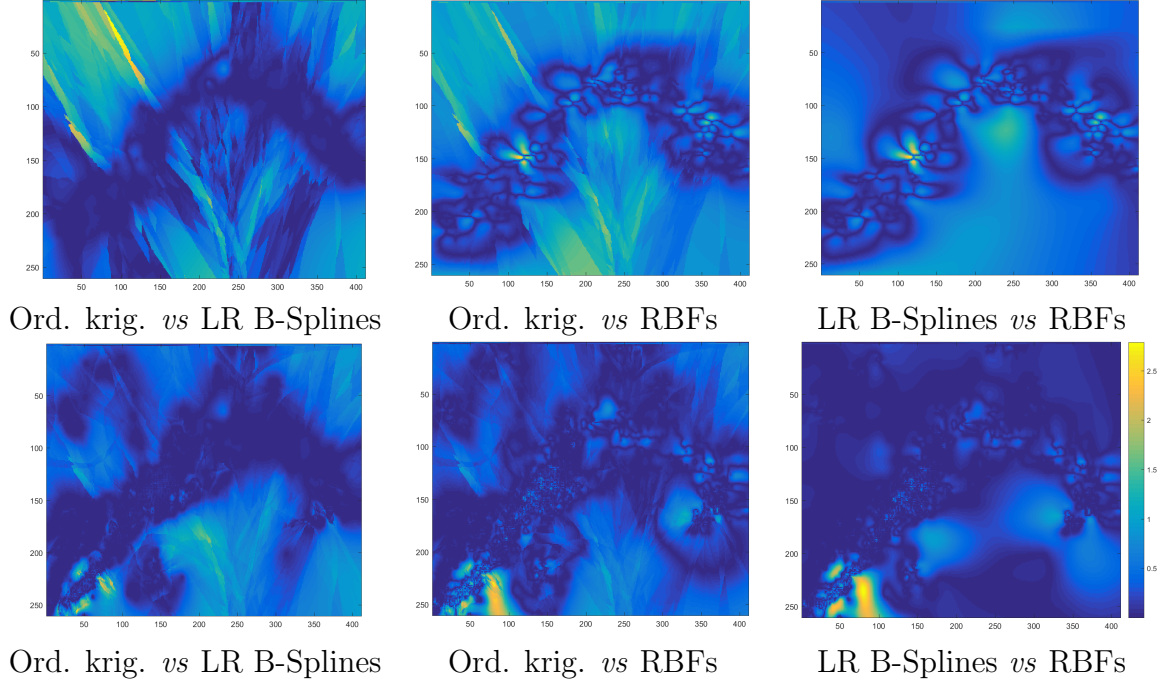


Figure 10: Point-wise difference of the rainfall fields evaluated on the rain stations (first row) and integrated the radar data (second row). Colors represent the difference from low (blue) to high (yellow) values.

a persistence threshold  $\varepsilon$ , namely  $\varepsilon = \tau(\max F - \min F)$  with  $\tau = 0.05, 0.15, 0.25, 0.35$ . In practice, a maximum is preserved only if its persistence is larger than  $\varepsilon$ , while the others are filtered away. Table 3 reports the total number of extracted persistent maxima, averaged by the amount of considered cumulative steps on the rainfall fields approximated from the rainfall stations only. Table 4 shows the maximum number of local maxima that have been extracted, method by method, from the 48 fields. Despite some slight differences in the results, the general trend is to have a decreasing number of persistent maxima as the threshold  $\tau$  increases. This situation is actually not surprising, since a higher persistence threshold implies that a larger portion of local maxima are pruned out. Also, for low values of the persistence threshold, we can relate the number of detected maxima to the smoothness of the considered approximation: in this view, the RBF schema appears to have a higher smoothing effect, as indicated by the smaller number of maxima characterized by a low persistence value.

Similarly, Tables 5 and 6 report the same data when the approximation schema integrate also the radar data. The trend to have a decreasing number of persistent

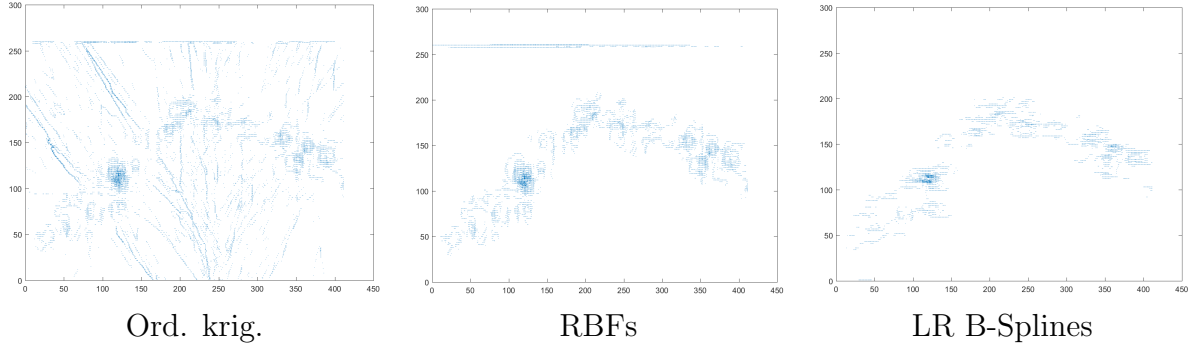


Figure 11: Gradient field of the three methods; in these images, the fields are approximated only with the rain stations.

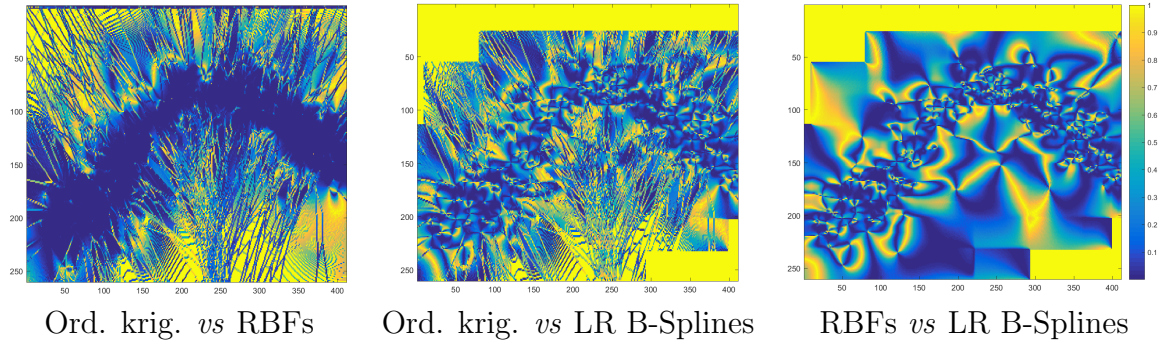


Figure 12: Local difference of the gradients of the three fields; colors represent the value of the distance  $d$  over the model grid from 0 (blue) to 1 (yellow).

maxima as the threshold  $\tau$  increases is confirmed and much more evident. Indeed, the approximation of the fields with such a higher number of constraints introduces a quite large number of local maxima that are not really relevant and that are discarded when the persistence threshold increases. Our tests further confirm that the RBF schemes generally have a higher smoothness, as indicated by the slightly smaller number of maxima.

### 6.1. Comparing sets of persistent maxima

In order to refine the above comparative analysis, we use the tracking procedure introduced in (Biasotti et al., 2015) to quantitatively assess a (dis)similarity measure between two sets of local maxima, originated from the three approximation schema. Data are considered the same cumulative step. Before presenting results, we briefly summarize the main ideas of (Biasotti et al., 2015).

Table 3: Statistics for the average number of extracted persistent maxima.

Method	$\tau = 0.05$	$\tau = 0.15$	$\tau = 0.25$	$\tau = 0.35$
Ord. krig.	28.31	11.27	6.70	4.37
RBFs	18.54	10.31	6.12	4.08
LR B-Splines	20.54	12.50	7.41	4.67

Table 4: Statistics for the maximum number of extracted persistent maxima.

Method	$\tau = 0.05$	$\tau = 0.15$	$\tau = 0.25$	$\tau = 0.35$
Ord. krig.	48	19	13	9
RBFs	26	17	11	9
LR B-Splines	28	18	13	10

For two sets  $\mathcal{F}, \mathcal{G}$  of local maxima of two rainfall fields  $F, G : \mathcal{M} \rightarrow \mathbb{R}$ , it is possible to compare them by measuring the cost of moving the points associated with one function to those of the other one, with the requirement that the longest of the transportations should be as short as possible. Interpreting the local maxima in  $\mathcal{F}$  and  $\mathcal{G}$  as points in  $\mathbb{R}^3$  (i.e., geographical position and persistence value), the collections of local maxima are compared through the *bottleneck distance* between  $\mathcal{F}$  and  $\mathcal{G}$ , which is defined as  $d_B(\mathcal{F}, \mathcal{G}) = \inf_{\gamma} \sup_{\mathbf{p}} d(\mathbf{p}, \gamma(\mathbf{p}))$ , where  $\mathbf{p} \in \mathcal{F}$ ,  $\gamma$  ranges over all the bijections between  $\mathcal{F}$  and  $\mathcal{G}$ ,  $d(\cdot, \cdot)$  is the *pseudo-distance*

$$d(\mathbf{p}, \mathbf{q}) := \min\{\|\mathbf{p} - \mathbf{q}\|, \max\{\text{pers}_F(\mathbf{p}), \text{pers}_G(\mathbf{q})\}\},$$

which measures the cost of moving  $\mathbf{p}$  to  $\mathbf{q}$ , and  $\|\cdot\|$  is a weighted modification of the Euclidean distance. In practice, the cost of taking  $\mathbf{p}$  to  $\mathbf{q}$  is measured as the minimum between the cost of moving one point onto the other and the cost of moving both points onto the plane  $xy : z = 0$ . Matching a point  $\mathbf{p}$  with a point of  $xy$ , which can be interpreted as the annihilation of  $\mathbf{p}$ , is allowed by the fact that the number of points for  $\mathcal{F}$  and  $\mathcal{G}$  is usually different. The matching  $\gamma$  between the points of  $\mathcal{F}$  and those of  $\mathcal{G}$ , for which  $d_B$  is actually occurred, is referred to as a *bottleneck matching* (Fig. 13). Through the bottleneck matching and the bottleneck distance, it is then possible to derive quantitative information about the differences in the spatial arrangement and the rain measurements for the points in  $\mathcal{F}$  and  $\mathcal{G}$ .

The bottleneck distance can be evaluated by applying a pure graph-theoretic approach or by taking into account geometric information that characterizes the assignment problem. We opt for a graph-theoretic approach, which is independent of any geometric constraint, and our implementation is based on the push-relabel maximum flow algorithm (Cherkassky and Goldberg, 1997). For each iteration, the

Table 5: Statistics for the average number of extracted persistent maxima with radar data.

<b>Method</b>	$\tau = \mathbf{0.05}$	$\tau = \mathbf{0.15}$	$\tau = \mathbf{0.25}$	$\tau = \mathbf{0.35}$
Ord. krig.	99.22	26.46	10.91	5.15
RBFs	93.35	24.85	9.85	4.68
LR B-Splines	113.46	31.58	13.05	6.33

Table 6: Statistics for the maximum number of extracted persistent maxima with radar data.

<b>Method</b>	$\tau = \mathbf{0.05}$	$\tau = \mathbf{0.15}$	$\tau = \mathbf{0.25}$	$\tau = \mathbf{0.35}$
Ord. krig.	175	62	27	13
RBFs	165	60	24	11
LR B-Splines	195	76	35	19

algorithm runs in  $O(k^{2.5})$ , where  $k$  is the number of local maxima involved in the comparison. We note that the computational complexity is not an issue, because the number of points to be considered is very limited in general. For example, in tracking applications the number of persistent maxima to be monitored is usually no more than a dozen for each time sample.

*Experimental results.* For each cumulative step, we consider the rainfall fields interpolated by the three methods, and extract the sets of local maxima according to the four persistence thresholds discussed above. For each threshold, the three collections of persistent maxima are pairwise compared as follows. Since geographic coordinates and rainfall measurements come with different reference frames and at different scales, local maxima to be matched are first normalized so that their coordinates range in  $[0,1]$ ; then, they are processed by computing the associated bottleneck matching and the bottleneck distance, and afterwards projected back in the original reference frames. Finally, a measure of their distance in terms of both geographical coordinates and rainfall values is derived by combining the information contained in the bottleneck matching and the associated numerical (dis)similarity score. Precisely, we consider the *geographical* and *rainfall distances*, which are defined as the largest difference in geographical position and rainfall value, respectively, for two persistent maxima that have been paired by the bottleneck matching.

Tables 7 and 8 report the obtained results, in terms of geographical and rainfall distances, respectively, averaged by the total number of considered cumulative steps. To have a clearer picture of the comparative evaluation in terms of the two distances, these results should be jointly interpreted for each persistence threshold. For instance, when  $\tau = 0.05$  we have (relatively) high values for the geographical distance together with quite low rainfall distance values: this can be interpreted as slight

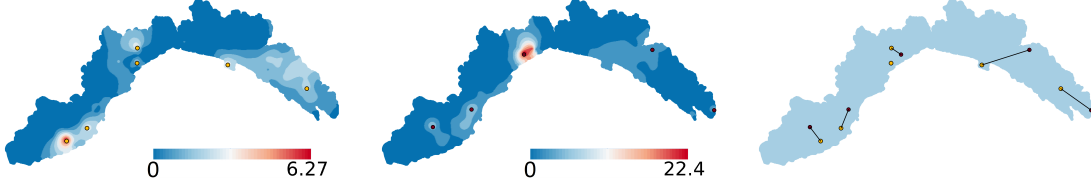


Figure 13: Two fields  $F, G : \mathcal{M} \rightarrow \mathbb{R}$ , color-coded from blue (low) to red (high) values, and the associated local maxima. On the right, bottleneck matching between local maxima.

Table 7: Average geographical distance (Km) between sets of local maxima (Liguria area size:  $5.410Km^2$ ).

Method1/Method2	$\tau = 0.05$	$\tau = 0.15$	$\tau = 0.25$	$\tau = 0.35$
Ord. krig / RBFs.	71.19 Km	13.76 Km	4.67 Km	2.46 Km
RBFs / LR B Spline	81.85 Km	54.47 Km	28.79 Km	14.46 Km
krig / LR B-Splines	104.59 Km	52.42 Km	29.66 Km	25.45 Km
Ord. krig + radar/ RBFs. + radar	186.01 Km	135.04 Km	7.27 Km	4.94 Km
RBFs + radar / LR B Spline + radar	223.89 Km	150.99 Km	23.20 Km	6.21 Km
krig + radar/ LR B-Splines + radar	121.49 Km	60.99 Km	30.10 Km	11.79 Km

numerical variations for the three approximations, possibly appearing spatially far one from each other. From this perspective, approximations with RBFs and kriging have an analogous behavior, both producing higher values for the geographical and rainfall distances when compared with LR-B Splines. Moving to higher persistence thresholds, the values of the geographical distance decrease, as an effect of filtering out non-relevant maxima, and the corresponding rainfall distance values reveal now the differences occurring at prominent maxima, which appear to be quite small.

We conclude by proposing in Table 9 a similar comparison of the results obtained when rainfall fields are interpolated by considering either observed rainfall measurements or an integration of these data with radar acquisitions (Sect. 5). Integrated data can reveal useful information for rainfall tracking over time, as a matter of the higher spatial and temporal resolution of radar data with respect to point-wise rainfall fields measured by instruments at the ground level. Although rainfall measurements are more reliable, integrating them with radar data makes it possible to extend the rainfall field interpolation in larger areas and to have a clearer picture about the temporal evolution of the associated precipitation event. According to the results in Table 9, which are characterized by high values in both the geographic and the rainfall distance, radar data can sensibly change the spatial location and the rainfall value of persistent maxima. This result can be interpreted as the intro-

Table 8: Average rainfall distance ( $mm$ ) between sets of local maxima.

<b>Method1/Method2</b>	$\tau = \mathbf{0.05}$	$\tau = \mathbf{0.15}$	$\tau = \mathbf{0.25}$	$\tau = \mathbf{0.35}$
Ord. krig / RBFs.	3.83 mm	1.87 mm	1.15 mm	0.28 mm
RBFs / LR B Sp.	3.21 mm	3.13 mm	3.10 mm	2.13 mm
Krig. / LR B-Sp.	3.63 mm	3.32 mm	2.63 mm	1.74 mm
Ord. krig + radar / RBFs. + radar	10.22 mm	7.39 mm	4.22 mm	1.47 mm
RBFs + radar / LR B Sp. + radar	11.38 mm	10.22 mm	8.86 mm	5.79 mm
Krig. + radar / LR B-Sp. + radar	11.35 mm	9.80 mm	8.52 mm	5.18 mm

Table 9: Average geographical ( $Km$ ) and rainfall distance ( $mm$ ) between sets of local maxima.

<b>Krig/ (Radar + Krig)</b>	$\tau = \mathbf{0.05}$	$\tau = \mathbf{0.15}$	$\tau = \mathbf{0.25}$	$\tau = \mathbf{0.35}$
Geogr. dist.	146.08 Km	100.68 Km	104.25 Km	83.48 Km
Rainfall dist.	17.52 mm	17.23 mm	16.90 mm	16.04 mm
<b>RBF/ (Radar + RBF)</b>	$\tau = \mathbf{0.05}$	$\tau = \mathbf{0.15}$	$\tau = \mathbf{0.25}$	$\tau = \mathbf{0.35}$
Geogr. dist.	95.38 Km	96.13 Km	93.29 Km	88.88 Km
Rainfall dist.	17.71 mm	17.25 mm	16.56 mm	16.21 mm
<b>LR B-spline/ ((Radar +LR B-Spline))</b>	$\tau = \mathbf{0.05}$	$\tau = \mathbf{0.15}$	$\tau = \mathbf{0.25}$	$\tau = \mathbf{0.35}$
Geogr. dist.	93.53 Km	94.72 Km	86.56 Km	77.09 Km
Rainfall dist.	18.77 mm	18.26 mm	17.953 mm	16.74 mm

duction of complementary information with respect to rainfall measurements, which hopefully support a clearer understanding of precipitation events.

## 7. Conclusions and future work

The aim of this study was the comparison of different spatial approximation methods finalized to compute the amount of rainfalls for hydro-metereological analysis and civil protection. For the approximation of rainfall data all the three approaches provide satisfactory results, with a preference for LR Splines and RBFs, and easily support the integration of further sources of rain measures, for instance those captured by radar.

As future work, we plan to proceed further with the presented comparison framework, including several more aspects and extending the evaluation to more elaborate correlation analysis, taking into account other relevant data, such as terrain morphology, satellite imagery, and meteorological situation. We will further investigate

this possibility and especially the effect on approximation results on storm tracking.

## Acknowledgments

This work has been supported by the FP7 Integrated Project IQmulus, FP7-ICT-2011-318787. The rainfall data sets are courtesy of ARPAL, Regione Liguria, and of the Genova Municipality.

## References

- Aronszajn, N., 1950. Theory of reproducing kernels. *Trans. of the American Mathematical Society* 68, 337–404.
- Azimi-Zonooz, A., Krajewski, W., Bowles, D., Seo, D., 1989. Spatial rainfall estimation by linear and non-linear co-kriging of radar-rainfall and raingage data. *Stochastic Hydrology and Hydraulics* 3 (1), 51–67.
- Biasotti, S., Cerri, A., Pittaluga, S., Sobrero, D., Spagnuolo, M., 2015. Persistence-based tracking of rainfall field maxima, topology-Based Methods in Visualization 2015, In press.
- Biasotti, S., Patanè, G., Spagnuolo, M., Falcidieno, B., 2007. Analysis and comparison of real functions on triangulated surfaces. *Curve and Surface Fitting Modern Methods in Mathematics*, 41–50.
- Brocca, L., Ciabatta, L., Massari, C., Moramarco, T., Hahn, S., Hasenauer, S., Kidd, R., Dorigo, W., Wagner, W., Levizzani, V., 2014. Soil as a natural rain gauge: Estimating global rainfall from satellite soil moisture data. *Journal of Geophysical Research: Atmospheres* 119 (9), 5128–5141.
- Carr, J. C., Beatson, R. K., Cherrie, J. B., Mitchell, T. J., Fright, W. R., McCallum, B. C., Evans, T. R., 2001. Reconstruction and representation of 3D objects with radial basis functions. In: *ACM Siggraph*. pp. 67–76.
- Cherkassky, B. V., Goldberg, A. V., 1997. On Implementing the Push-Relabel Method for the Maximum Flow Problem. *Algorithmica* 19 (4), 390–410.
- Creutin, J., Delrieu, G., Lebel, T., 1988. Rain measurement by raingage-radar combination: a geostatistical approach. *Journal of Atmospheric and Oceanic Technology* 5 (1), 102–115.

- Dey, T. K., Sun, J., 2005. An adaptive MLS surface for reconstruction with guarantees. In: ACM Symposium on Geometry Processing. pp. 43–52.
- Di Piazza, A., Conti, F., Noto, L., Viola, F., La Loggia, G., 2011. Comparative analysis of different techniques for spatial interpolation of rainfall data to create a serially complete monthly time series of precipitation for sicily, italy. *International Journal of Applied Earth Observation and Geoinformation* 13 (3), 396–408.
- Dixon, M., Wiener, G., 1993. Titan: Thunderstorm identification, tracking, analysis, and nowcasting—a radar-based methodology. *Journal of Atmospheric and Oceanic Technology* 10 (6), 785–797.
- Dokken, T., Lyche, T., Pettersen, K. F., 2013. Polynomial splines over locally refined box-partitions. *Computer Aided Geometric Design* 30 (3), 331–356.
- Dyn, N., Levin, D., Rippa, S., 1986. Numerical procedures for surface fitting of scattered data by radial functions. *SIAM Journal on Scientific and Statistical Computing* 7(2), 639–659.
- Edelsbrunner, H., Harer, J., 2010. *Computational Topology: An Introduction*. American Mathematical Society.
- Edelsbrunner, H., Letscher, D., Zomorodian, A., 2002. Topological persistence and simplification. *Discrete Computational Geometry* 28, 511–533.
- Farr, T. G., Rosen, P. A., Caro, E., Crippen, R., Duren, R., Hensley, S., Kobrick, M., Paller, M., Rodriguez, E., Roth, L., 2007. The shuttle radar topography mission. *Reviews of Geophysics* 45 (2), 361–363.
- Goovaerts, P., 1997. *Geostatistics for natural resources evaluation*. Oxford University Press.
- Goovaerts, P., 2000. Geostatistical approaches for incorporating elevation into the spatial interpolation of rainfall. *Journal of Hydrology* 228 (1), 113–129.
- Han, L., Fu, S., Zhao, L., Zheng, Y., Wang, H., Lin, Y., 2009. 3D Convective Storm Identification, Tracking, and Forecasting—An Enhanced TITAN Algorithm. *Journal of Atmospheric and Oceanic Technology* 26 (4), 719–732.
- Hong, Y., Adler, R., Huffman, G., 2007. An experimental global prediction system for rainfall-triggered landslides using satellite remote sensing and geospatial datasets. *IEEE Trans. on Geoscience and Remote Sensing* 45 (6), 1671–1680.



- Hou, A. Y., Ramesh, K. K., Neeck, S., Azarbarzin, A. A., Kummerow, C. D., Kojima, M., Oki, R., Nakamura, K., Iguchi, T., 2014. The global precipitation measurement mission. *Bulletin of the American Meteorological Society* 95.
- Journel, A. G., Huijbregts, C. J., 1978. *Mining geostatistics*. Academic press.
- Keefer, D., Wilson, R., Mark, R., Brabb, E., Brown, W., Ellen, S., Harp, E., Wiczorek, G., Alger, C., Zatkin, R., 1987. Real-time landslide warning during heavy rainfall. *Science* 238, 921–925.
- Kucera, P. A., Ebert, E. E., Turk, F. J., Levizzani, V., Kirschbaum, D., Tapiador, F. J., Loew, A., Borsche, M., 2013. Precipitation from space: advancing earth system science. *Bulletin of the American Meteorological Society* 94, 365–375.
- Lakshmanan, V., Smith, T., 2009. An Objective Method of Evaluating and Devising Storm-Tracking Algorithms. *Wea. Forecasting* 25 (2), 701–709.
- Lee, S., Wolberg, G., Shin, S. Y., 1997. Scattered data interpolation with multilevel b-splines. *IEEE Trans. on Visualization and Computer Graphics* 3 (3), 228–244.
- McCuen, R. H., 1989. *Hydrologic analysis and design*. Prentice-Hall Englewood Cliffs, NJ.
- McRobie, F. H., Wang, L.-P., Onof, C., Kenney, S., 2013. A spatial-temporal rainfall generator for urban drainage design. *Water Science and Technologies* 68 (1), 240–249.
- Micchelli, C. A., 1986. Interpolation of scattered data: Distance matrices and conditionally positive definite functions. *Constructive Approximation* 2, 11–22.
- Mitra, N. J., Nguyen, A., 2003. Estimating surface normals in noisy point cloud data. In: *Proc. of Computational Geometry*. ACM Press, pp. 322–328.
- Morse, B. S., Yoo, T. S., Chen, D. T., Rheingans, P., Subramanian, K. R., 2001. Interpolating implicit surfaces from scattered surface data using compactly supported radial basis functions. In: *IEEE Shape Modeling and Applications*. pp. 89–98.
- Patanè, G., Spagnuolo, M., Falcidieno, B., 2009. Topology- and error-driven extension of scalar functions from surfaces to volumes. *ACM Trans. on Graphics* 29 (1), 1–20.

- Saupe, D., 1988. Algorithms for random fractals. In: The science of fractal images. Springer, pp. 71–136.
- Scheuerer, M., Schaback, R., Schlather, M., 2013. Interpolation of spatial data - a stochastic or a deterministic approach? *European Journal of Applied Mathematics* 24, 601–629.
- Segond, M.-L., 2007. The significance of spatial rainfall representation for flood runoff estimation: A numerical evaluation based on the Lee catchment. *Journal of Hydrology* 347, 116 – 131.
- Skok, G., Vrhovec, T., 2006. Considerations for interpolating rain gauge precipitation onto a regular grid. *Meteorologische Zeitschrift* 15 (5), 545–550.
- Teegavarapu, R. S. V., Chandramouli, V., 2005. Improved weighting methods, deterministic and stochastic data-driven models for estimation of missing precipitation records. *Journal of Hydrology* 312 (1), 191–206.
- Thiessen, A. H., 1911. Precipitation averages for large areas. *Monthly weather review* 39 (7), 1082–1089.
- Turk, G., O’Brien, J. F., 2002. Modelling with implicit surfaces that interpolate. *ACM Siggraph* 21 (4), 855–873.
- Wackernagel, H., 2003. *Multivariate geostatistics: an introduction with applications*, 2nd Edition. Springer-Verlag.
- Wake, B., 2013. Flooding costs. *Nature Climate Change* 3 (9), 1671–1680.
- Wendland, H., 1995. Real piecewise polynomial, positive definite and compactly supported radial functions of minimal degree. *Advances in Computational Mathematics* 4(4), 389–396.
- Willems, P., 2001. A spatial rainfall generator for small spatial scales. *Journal of Hydrology* 252, 126 – 144.

**Recent titles from the IMATI-REPORT Series:**

- 16-01:** *Optimal strategies for a time-dependent harvesting problem*, G.M. Coclite, M. Garavello, L.V. Spinolo.
- 16-02:** *A new design for the implementation of isogeometric analysis in Octave and Matlab: GeoPDEs 3.0*, R. Vázquez.
- 16-03:** *Defect detection in nanostructures*, D. Carrera, F. Manganini, G. Boracchi, E. Lanzarone.
- 16-04:** *A study of the state of the art of process planning for additive manufacturing*, M. Livesu, M. Attene, M. Spagnuolo, B. Falcidieno.
- 16-05:** *Calcolo di descrittori ibridi geometria-colore per l'analisi di similarità di forme 3D*, A. Raffo, S. Biasotti.
- 16-06:** *An appointment scheduling framework to balance the production of blood bags from donation*, S. Baş, G. Carello, E. Lanzarone, S. Yalçındağ.
- 16-07:** *From lesson learned to the refactoring of the DRIHM science gateway for hydro-meteorological research*, D. D'Agostino, E. Danovaro, A. Clematis, L. Roverelli, G. Zereik, A. Galizia.
- 16-08:** *Algorithms for the implementation of adaptive isogeometric methods using hierarchical splines*, E.M. Garau, R. Vázquez.
- 16-09:** *Feature curve identification in archaeological fragments using an extension of the Hough transform*, M.L. Torrente, S. Biasotti, B. Falcidieno.
- 16-10:** *Comparing methods for the approximation of rainfall fields in environmental applications*, G. Patané, A. Cerri, V. Skytt, S. Pittaluga, S. Biasotti, D. Sobrero, T. Dokken, M. Spagnuolo.